Available online at www.sciencedirect.com
SCIENCE DIRECT®
Journal of Sound and Vibration 270 (2004) 793–811
JOURNAL OF SOUND AND VIBRATION
www.elsevier.com/locate/jsvi

Effect of fluid wall shear stress on non-linear beam vibration

W. Buhler, A. Frendi*

Department of Mechanical and Aerospace Engineering, University of Alabama in Huntsville, N274 Technology Hall, Huntsville, AL 35899, USA

Received 17 June 2002; accepted 5 February 2003

Abstract

In this paper, the effects of tension and fluid wall shear stress on non-linear structural vibrations are investigated. Results show that fluid wall shear stress both suppresses and increases the non-linear response given by the large deflection response depending on its value. An in-depth analysis of the non-linear vibration response shows vibration energy flowing from the fundamental to the harmonics and then subharmonics as the excitation level increases. Various techniques to suppress non-linear vibrations were examined and most gave the same result, which is suppression of the subhramonics and harmonics.

1. Introduction

It is well known in structural dynamics that at high excitation levels, linear theory cannot be used to accurately predict structural response. For instance, linear plate theory used in sonic fatigue life predictions for aircraft structures subjected to high sound pressure levels, has led to poor results when compared to experimental data [1,2]. In order to overcome the weakness of linear theory, several non-linear models have been proposed. Mei and Prasad [3] used a non-linear damping model in an attempt to explain some experimental phenomena observed for aircraft panels excited by a high intensity sound. They found that non-linear damping contributed significantly to the broadening of the response peaks at high excitation levels. In another experimental and numerical study, Maestrello et al. [4] showed that when a flat panel was excited by plane acoustic waves having a frequency that corresponds to one of the panel's natural frequencies, its response became non-linear as the amplitude of the excitation was increased. Only few authors have studied the effect of the surrounding fluid on the response of a flexible structure. Frendi et al. [5] showed the existence of a strong coupling between plate vibration and the

*Corresponding author. Tel.: +1-256-824-7206; fax: +1-256-824-6758.
E-mail address: frendi@mae.uah.edu (A. Frendi).

0022-460X/03/$ - see front matter
doi:10.1016/S0022-460X(03)00258-X

surrounding flowfield at high excitation levels. However, in most structural vibration studies, fluid wall shear stress has been neglected. In this paper a non-linear model is used to investigate the effect of fluid wall shear stress on the non-linear structural vibrations of a beam and to test various techniques to suppress non-linear vibrations. For instance, it is well known that damping tape reduces the vibration levels of a structure. Maestrello et al. [6] observed experimentally that the non-linear plate response to a high acoustic excitation becomes linear when a damping tape or a shaker-type control is applied at the same frequency as that of the excitation but with an opposite phase. Keith and Bennett [7] made wall shear stress measurements in a fully developed turbulent boundary layer at Reynolds numbers of 8200 and 13 400 using a hot-film wall shear stress transducer. Chase [8] derived a semi-empirical model for the wavevector-frequency spectrum of turbulent wall shear stress. He found that the resulting computed spectral density at low wavenumbers was comparable to the experimental low-wavenumber turbulent wall pressure.

2. Formulation of the model

The physical problem addressed in this paper is that of non-linear beam vibrations. The governing differential equation describing the motion of the flexible beam shown in Fig. 1 is derived using Cauchy's first law of motion in undeformed Cartesian co-ordinates:

$$D\frac{\partial^4\eta}{\partial x^4} - \bar{N}_x\frac{\partial^2\eta}{\partial x^2} - \frac{\partial}{\partial x}\left[\tau_w\left(\eta + \frac{h}{2}\right)\right] + \rho_p h\frac{\partial^2\eta}{\partial t^2} + \Gamma\frac{\partial\eta}{\partial t} = \Delta p(t), \tag{1}$$

where η is the transverse beam deflection, τ_w is the fluid wall shear stress, $\rho_p h$ is the mass per unit area of the beam, h the beam thickness and Γ its physical damping. D is the stiffness defined as $D = Eh^3/12(1-\nu^2)$, with E being the modulus of elasticity in tension and ν the Poisson's ratio of the beam material. The coefficient $\bar{N}_x$ is given by

$$\bar{N}_x = \frac{Eh}{2L}\int_{x_0}^{x_0+L}\left(\frac{\partial\eta}{\partial x}\right)^2 \mathrm{d}x, \tag{2}$$

which characterizes the tension created by stretching of the beam due to bending, x_0 is the beam origin and L its length (see Fig. 1). The forcing term of Eq. (1), $\Delta p(t)$, is written as

$$\Delta p(t) = \varepsilon\sin(\omega t), \tag{3}$$

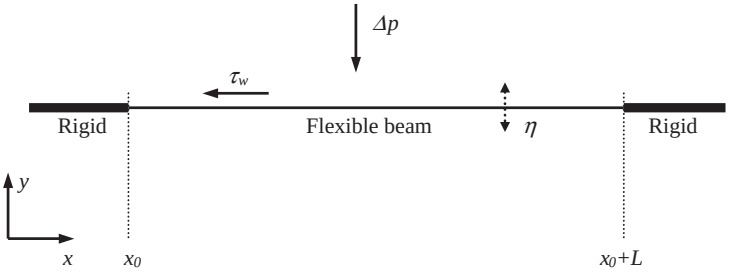

Fig. 1. Physical boundaries of the model.

with ω and ε being the forcing frequency and the excitation amplitude, respectively. Eqs. (1)–(3) are written in non-dimensional form with P_{ref}, $1/f$ and h as the reference quantities. The reference pressure is that of the air at sea-level conditions, which is $P_{ref} = 101\,326$ Pa, the beam thickness, which is the reference length, is $h = 0.508$ mm and the reference time is the inverse of the excitation frequency $f = 631$ Hz corresponding to the fifth mode of the beam. The non-dimensional results, designated by the star notation, are presented in this paper.

3. Methods of solution

The dynamic equations of motion (1)–(3) are solved using an implicit finite difference method for structural dynamics developed by Hoff and Pahl [9] known as the θ_1-method. Extension of the algorithm to Eq. (1) was developed by Buhler [10]. Numerical integration of $\bar{N}_x^*$ is achieved through a series of iterations within each time step using the Cubic Splines method [10]. The boundary conditions used to solve the non-linear beam equation are those of a clamped beam:

$$\eta(x) = \eta_{,x}(x) = 0, \quad \text{at } x = x_0 \text{ and } x = x_0 + L. \tag{4}$$

4. Results and discussion

The numerical experiments simulate the forced vibration of a beam. The beam properties are: thickness $h = 0.508$ mm, length $L = 254$ mm, stiffness $D = 2$ N m, mass per unit area $\rho_p h = 2.714$ kg/m^2, Poisson's ration $v = 0.3$ and physical damping $\Gamma = 1.520 \times 10^2$ N s/m^3. The first six natural frequencies of the beam are 47, 131, 256, 423, 631 and 824 Hz. An excitation frequency of 631 Hz is used in order to excite one resonant mode of the beam. The results will be divided into two groups; one in which only the effects of $\bar{N}_x^*$ on the response is studied and the other in which the combined effect of τ_w^* and $\bar{N}_x^*$ is studied. In the last section, results from the control of non-linear vibrations using different methods will be discussed.

4.1. Effects of $\bar{N}_x^*$ on the beam response

In this subsection, τ_w^* is set equal to zero. In order to study the effect of $\bar{N}_x^*$, the excitation amplitude is increased by small increments and a sequence of solutions is obtained.

For small amplitude forcing, $\varepsilon^* = 0.027$, the beam response is linear as shown in Fig. 2. The time history, Fig. 2(a), the PSD, Fig. 2(b), the phase diagram, Fig. 2(c) and the Poincaré map, Fig. 2(d), indicate that the response is indeed linear and harmonic. Increasing ε^* to 0.136 results in increased non-linear response, as shown in Fig. 3. An additional frequency can be observed in the displacement time history, Fig. 3(a), and the PSD, Fig. 3(b). The phase diagram, Fig. 3(c), shows the presence of two small loops on top of the main loop. This is confirmed by the Poincaré map, Fig. 3(d), which shows three attractors. The new frequency spike shown on the PSD corresponds to the $3f$ harmonic. There is no spike at the second harmonic, $2f$. We believe this is due to the absence of a symmetric mode in the vicinity of $2f$, while there is a symmetric mode near $3f$ [11].

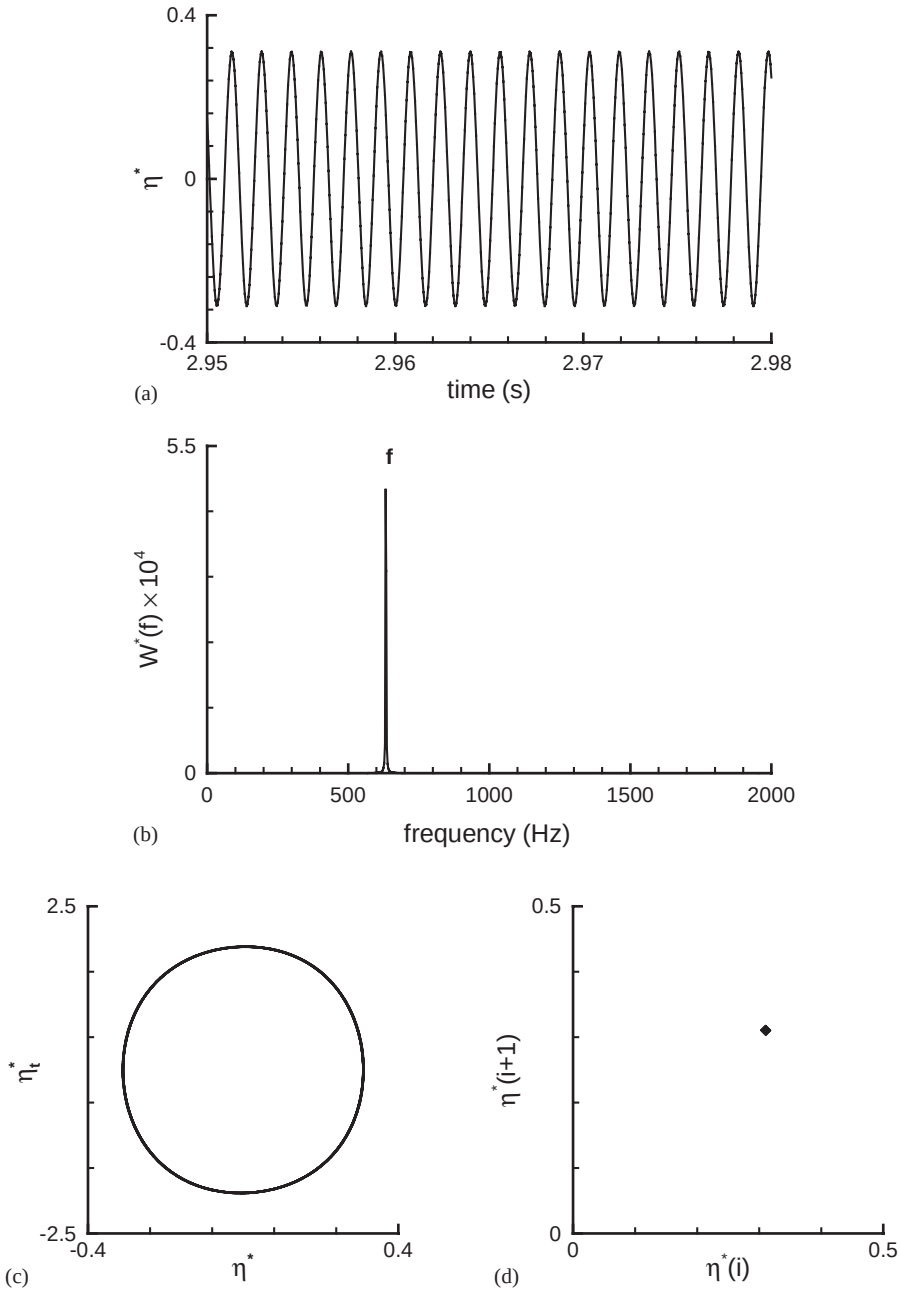

Fig. 2. Linear response of the beam center for $\varepsilon^* = 0.027$: (a) time history, (b) power spectral density (PSD), (c) phase diagram and (d) Poincaré map.

Increasing the value of the excitation amplitude to $\varepsilon^* = 0.197$ leads to a more complex dynamical behavior. There is no easily detectable periodicity in the time history, Fig. 4(a), however the phase diagram, Fig. 4(c), shows a relatively repetitive behavior despite its apparent

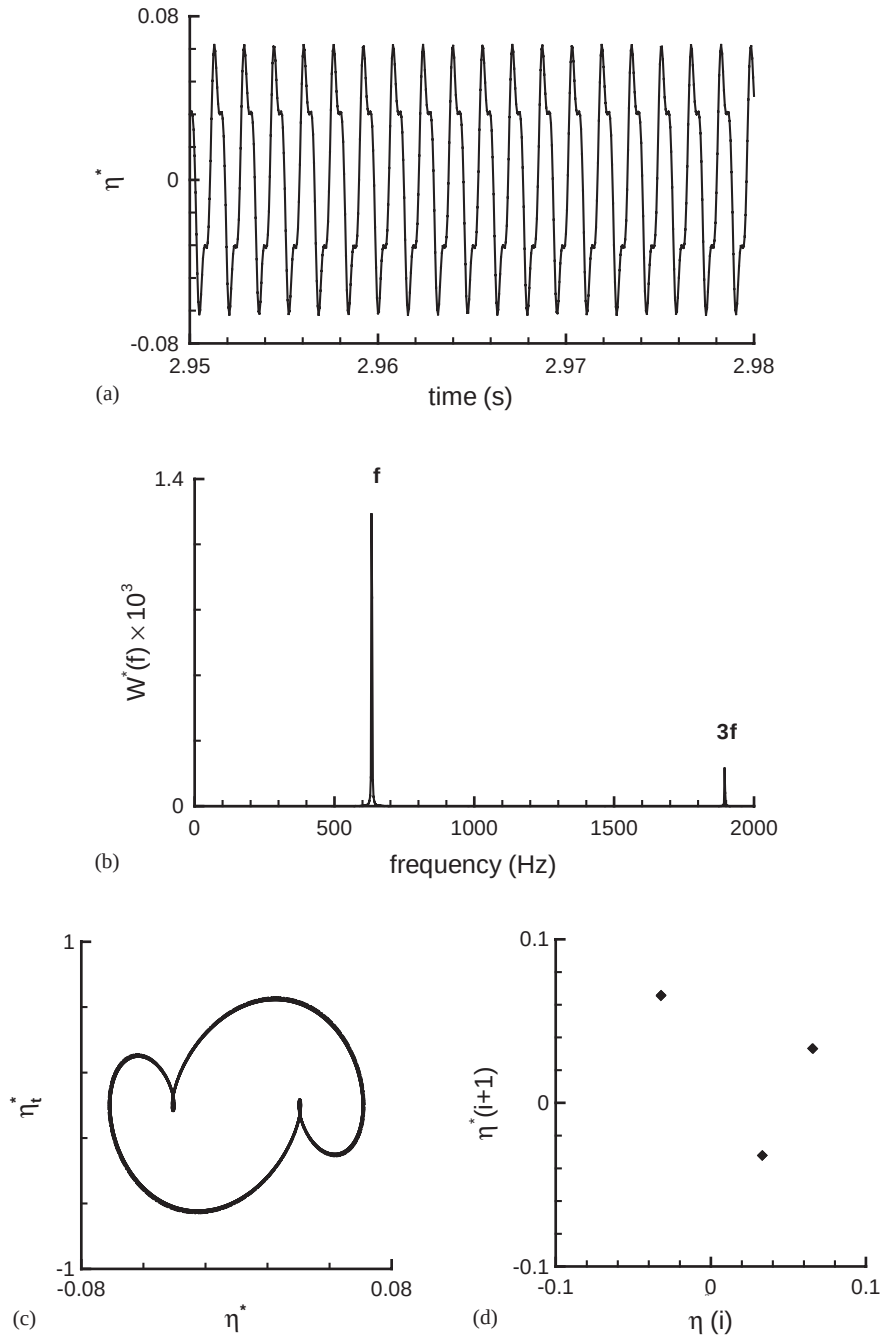

Fig. 3. Non-linear response of the beam center for $\varepsilon^* = 0.136$: (a) time history, (b) PSD, (c) phase diagram and (d) Poincaré map.

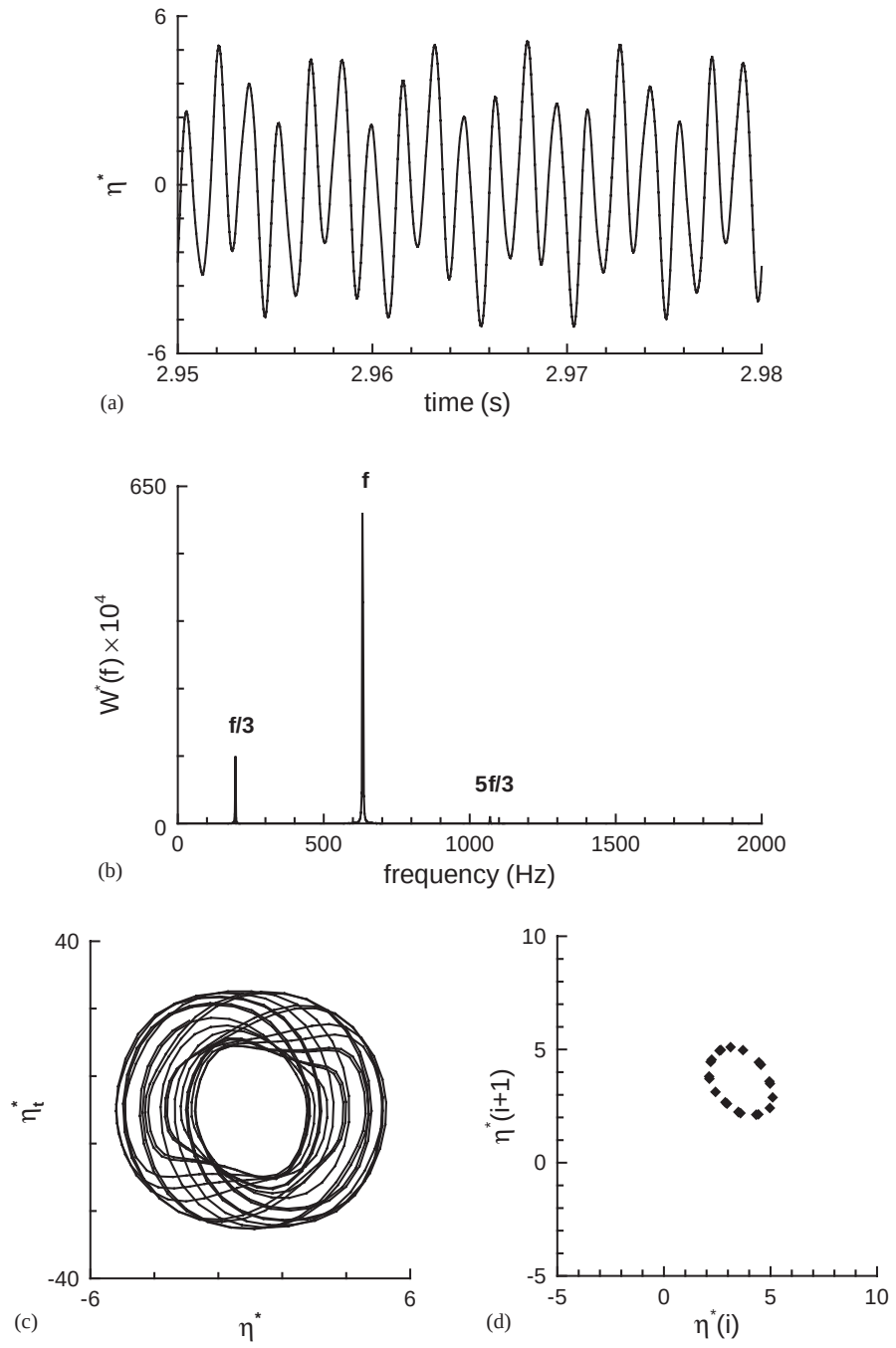

Fig. 4. Non-linear response of the beam center for $\varepsilon^* = 0.197$: (a) time history, (b) PSD, (c) phase diagram and (d) Poincaré map.

complex shape. This is confirmed by the corresponding Poincaré map, Fig. 4(d), which shows the presence of many attractors distributed along a circular path. Therefore the beam response is quasi-periodic. The PSD, Fig. 4(b), shows the presence of two new spectral peaks in addition to the fundamental. One is a subharmonic very close to the $f/3$ frequency and the other is a harmonic of the subharmonic corresponding to $5f/3$. The contribution to this harmonic is however very weak contrary to the subharmonic.

When ε^* is increased further to 0.201, Fig. 5, the $f/3$ subharmonic becomes larger in amplitude than the fundamental, Fig. 5(b). The fundamental, in this case, can be thought of as the harmonic of $f/3$. The amplitude of the transverse displacement at the center of the beam, Fig. 5(a), is also larger than in the previous cases. The phase diagram, Fig. 5(c), shows three loops, which is consistent with the presence of a strong $f/3$ subharmonic and the three attractors of the Poincaré map, Fig. 5(d).

In an attempt to understand the vibration energy transfer phenomena between the various frequencies, the distribution of the beam vibration energy as a function of frequency and excitation amplitude is shown in Fig. 6. The total energy contained in the PSD for each ε^* has been scaled to 1, with 1 being the amplitude of the energy contained in the response to an excitation with $\varepsilon^* = 0.204$. The figure shows that as ε^* increases, energy is transferred from the fundamental to the harmonics and then the subharmonics.

4.2. *Effect of the wall shear stress*

The influence of the wall shear stress on the solution is now studied. The wall shear stress is normally obtained from the flow solution [12], however for simplicity, in this study, the shear stress will be taken as a constant. Two values of ε^* are considered, $\varepsilon^* = 0.027$ and 0.197. These two excitation amplitudes resulted in a linear and a non-linear beam response, respectively, when the wall shear stress was neglected.

For $\varepsilon^* = 0.027$, a sequence of solutions is obtained for increasing values of wall shear stress. For relatively small values of wall shear stress ($\tau_w^* \leqslant 1.361$) the beam response remains linear. The case for $\tau_w^* = 1.361$ is illustrated in Fig. 7. The time history, Fig. 7(a), and the PSD, Fig. 7(b), indicate that the response is indeed linear. These results are expected since the value of the wall shear stress is small.

Increasing τ_w^* to 1.429 results in a complex dynamical response represented by an additional frequency in the PSD, Fig. 8(b). This additional frequency is close to the $f/4$ subharmonic. It is difficult to identify the periodicity in the time history, Fig. 8(a). However the phase diagram, Fig. 8(c), and the Poincaré map, Fig. 8(d), show that the response is quasi-periodic.

Fig. 9 illustrates the beam response for $\tau_w^* = 2.041$. The plots exhibit a dynamical response characteristic of a chaotic response. Additional peaks are formed in the PSD around $f/4$ and f, Fig. 9(b), suggesting a narrowband chaotic behavior. Even though its level has decreased, the fundamental is still dominant. This chaotic behavior is confirmed by the complexity of the phase diagram, Fig. 9(c), and the Poincaré map, Fig. 9(d). Contrary to the previous cases, there is no dominant attractor. The window in which such complex behavior exists is very small. Thus the beam response is very sensitive to the value of τ_w^* and a small variation in the wall shear stress leads to a totally different response, as shown in Fig. 10 obtained for $\tau_w^* = 2.381$.

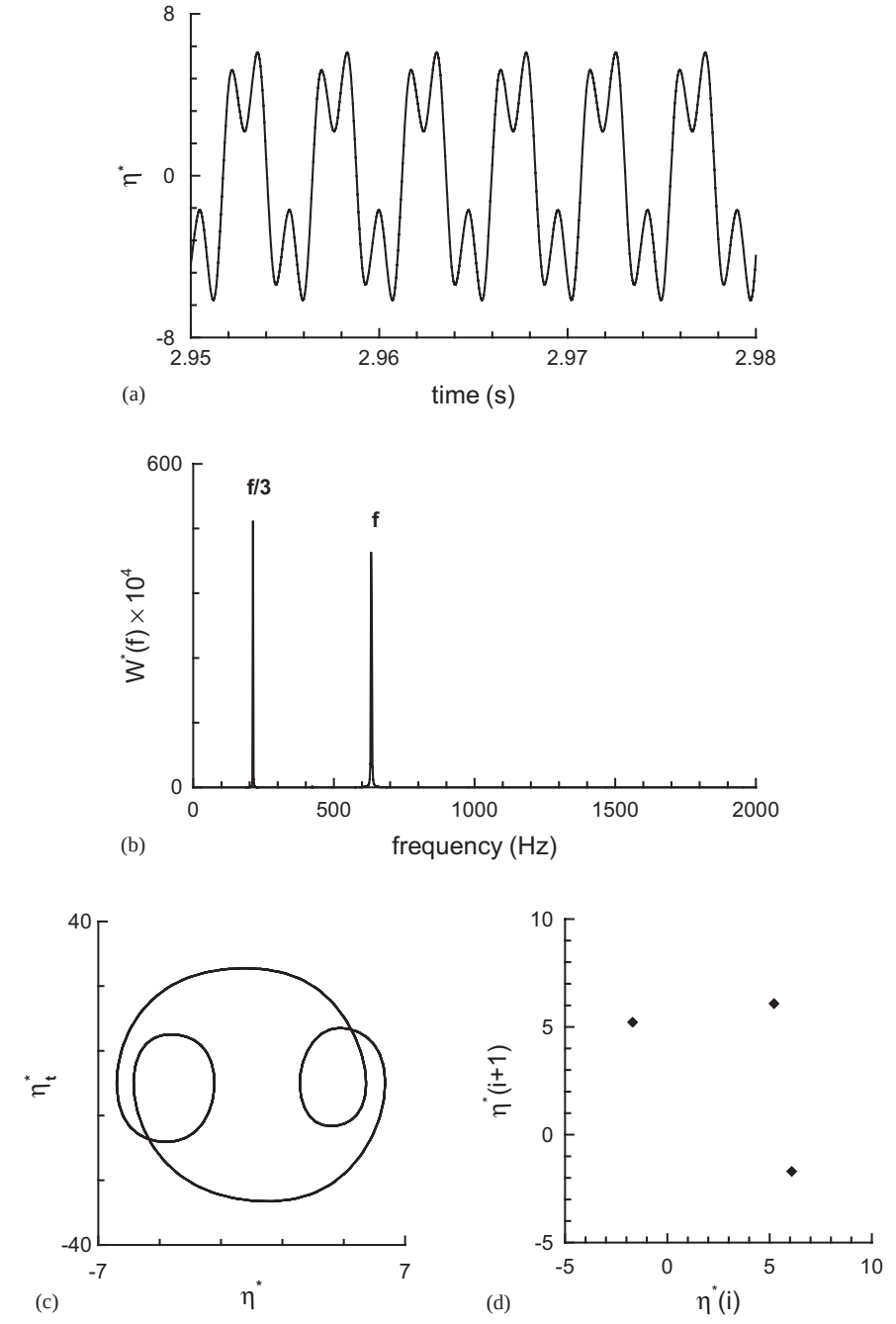

Fig. 5. Non-linear response of the beam center for $\varepsilon^* = 0.201$: (a) time history, (b) PSD, (c) phase diagram and (d) Poincaré map.

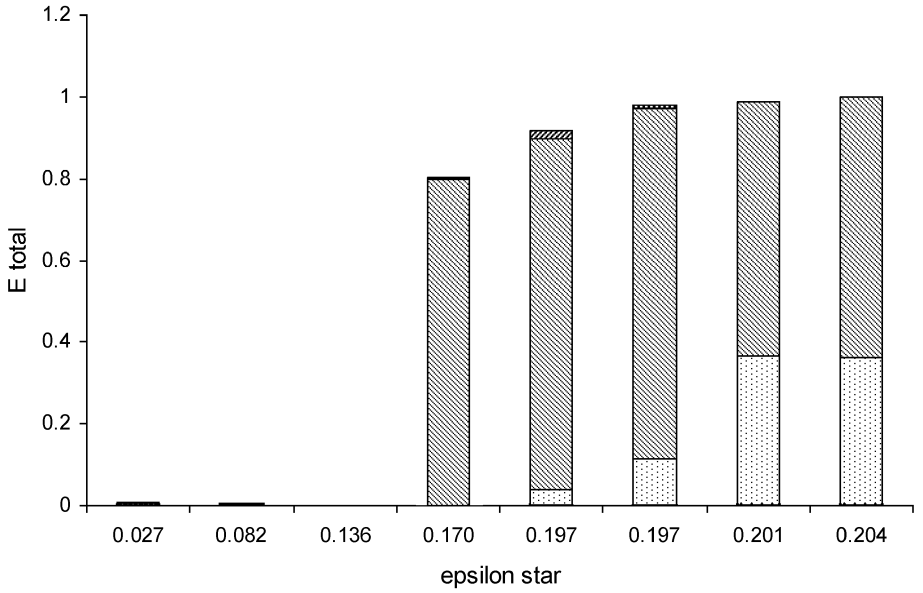

Fig. 6. Distribution of the vibration energy as a function of the frequency f and the excitation amplitude ε^*: □, $f/3$ (210 Hz); ▨, f (631 Hz); ■, $5f/3$ (1052 Hz).

The time history, Fig. 10(a), is periodic and shows three local maxima per cycle, in accordance with the three loops of the phase diagram, Fig. 10(c), and the three points of the Poincaré map, Fig. 10(d). Instead of the $f/4$ subharmonic obtained in previous cases, we now have an $f/3$ subharmonic that is stronger than the fundamental.

Results obtained for $\varepsilon^* = 0.197$ and for increasing values of wall shear stress are now presented. Contrary to the case shown in Fig. 4 for $\varepsilon^* = 0.197$ and $\tau_w^* = 0$, the response is linear-like for small shear stress values ($\tau_w^* \leqslant 0.136$). The $\tau_w^* = 0.136$ case is shown in Fig. 11, the time history, Fig. 11(a), and the PSD, Fig. 11(b), indicate that the response is indeed linear-like and periodic. This is confirmed by the phase diagram, Fig. 11(c), which is nearly circular, and the Poincaré map, Fig. 11(d), which reduces to a point. The wall shear stress has suppressed the subharmonics and the harmonic. Therefore a low wall shear stress can be used to suppress non-linear vibrations.

As τ_w^* is increased, more energy is added to the subharmonic, making the response more non-linear. As shown on the PSD of Fig. 12 for $\tau_w^* = 0.340$, the level of the subharmonic $f/3$ is higher than that of the fundamental. The phase diagram, Fig. 12(c), is now showing three loops, consistent with the three local maxima per cycle in the time history. Similarly, the Poincaré map, Fig. 12(d), shows three attractors. In this case, τ_w^* increases the level of non-linearity of the beam response.

4.3. Control of non-linear vibrations

Only one value of ε^* is considered throughout this subsection, $\varepsilon^* = 0.197$. This excitation amplitude resulted in a complex dynamical behavior when the wall shear stress was neglected. Three control techniques are used. A widely used passive control technique consists of applying damping tape at the edges of the beam. The consequence is an increase of Γ_t, the tape damping, to

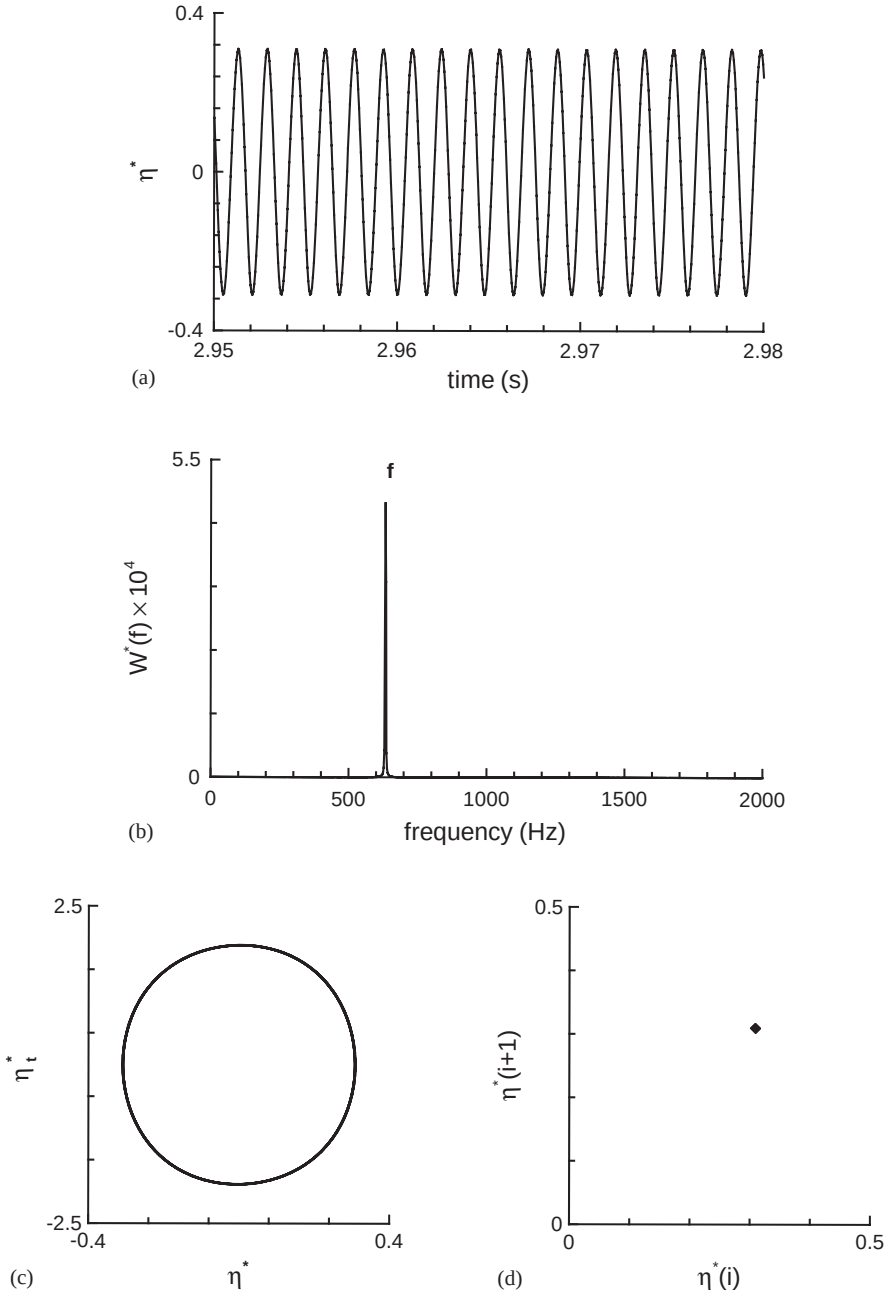

Fig. 7. Linear response of the beam center for $\varepsilon^* = 0.027$ and $\tau_w^* = 1.361$: (a) time history, (b) PSD, (c) phase diagram and (d) Poincaré map.

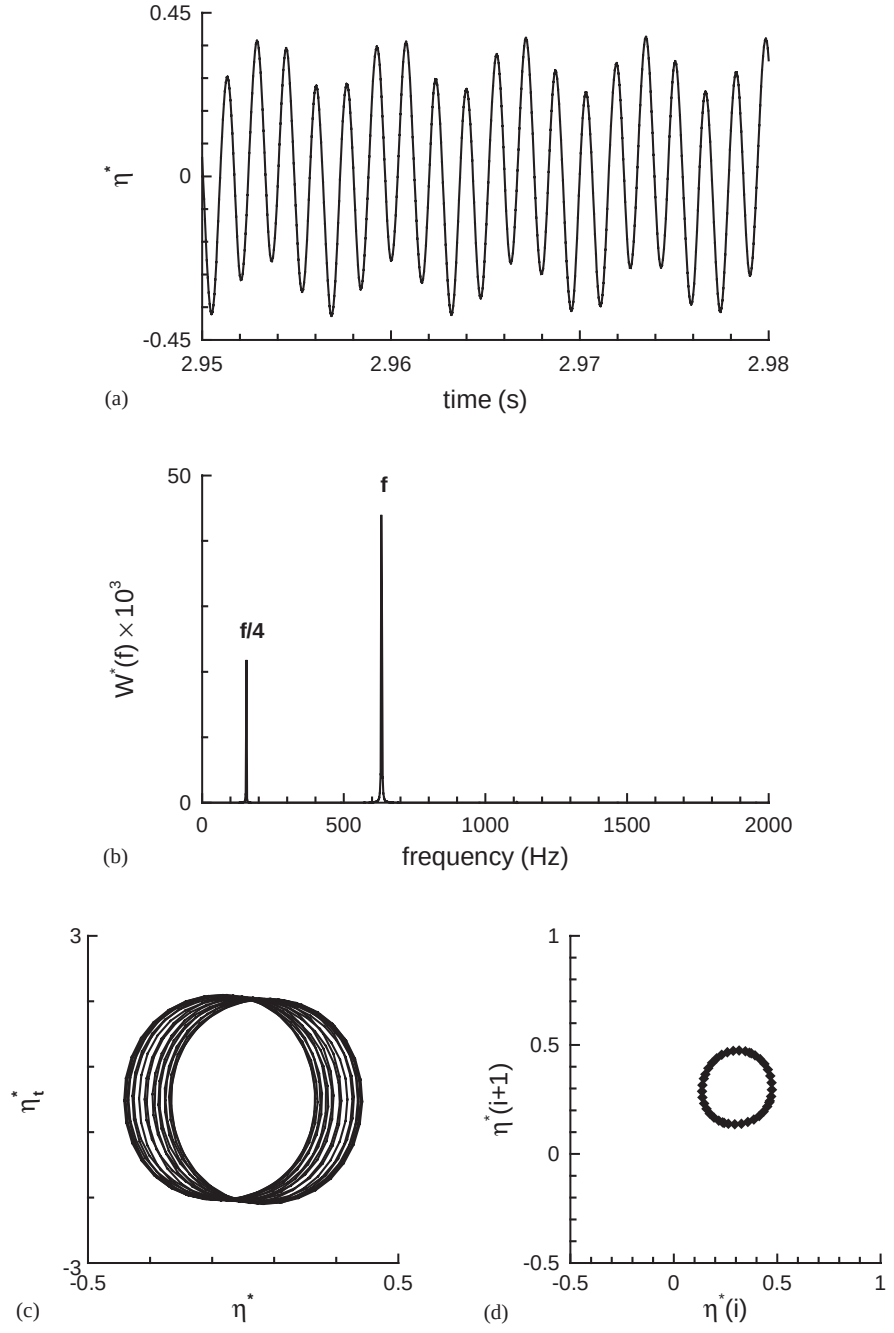

Fig. 8. Non-linear response of the beam center for $\varepsilon^* = 0.027$ and $\tau_w^* = 1.429$: (a) time history, (b) PSD, (c) phase diagram and (d) Poincaré map.

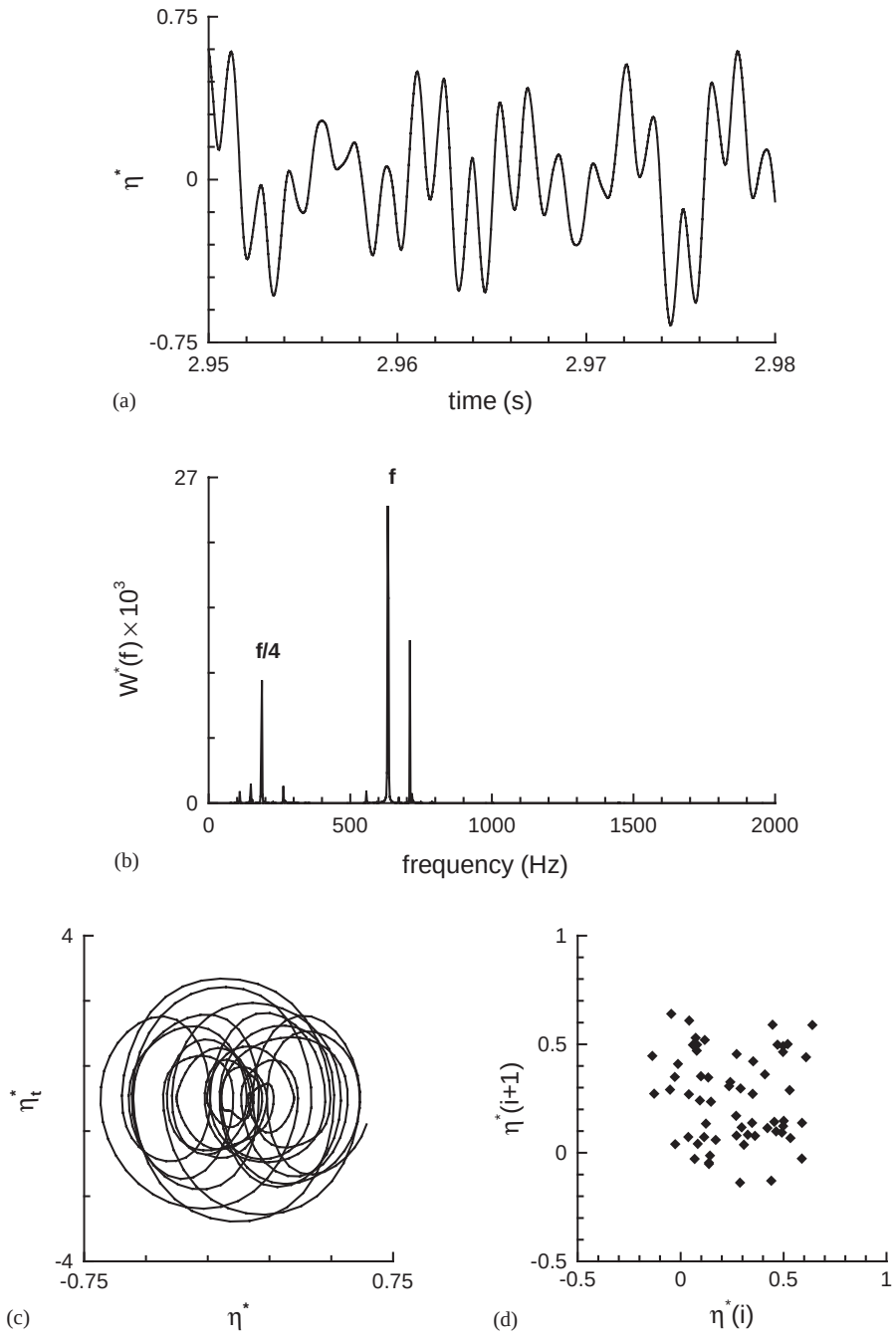

Fig. 9. Non-linear response of the beam center for $\varepsilon^* = 0.027$ and $\tau_w^* = 2.041$: (a) time history, (b) PSD, (c) phase diagram and (d) Poincaré map.

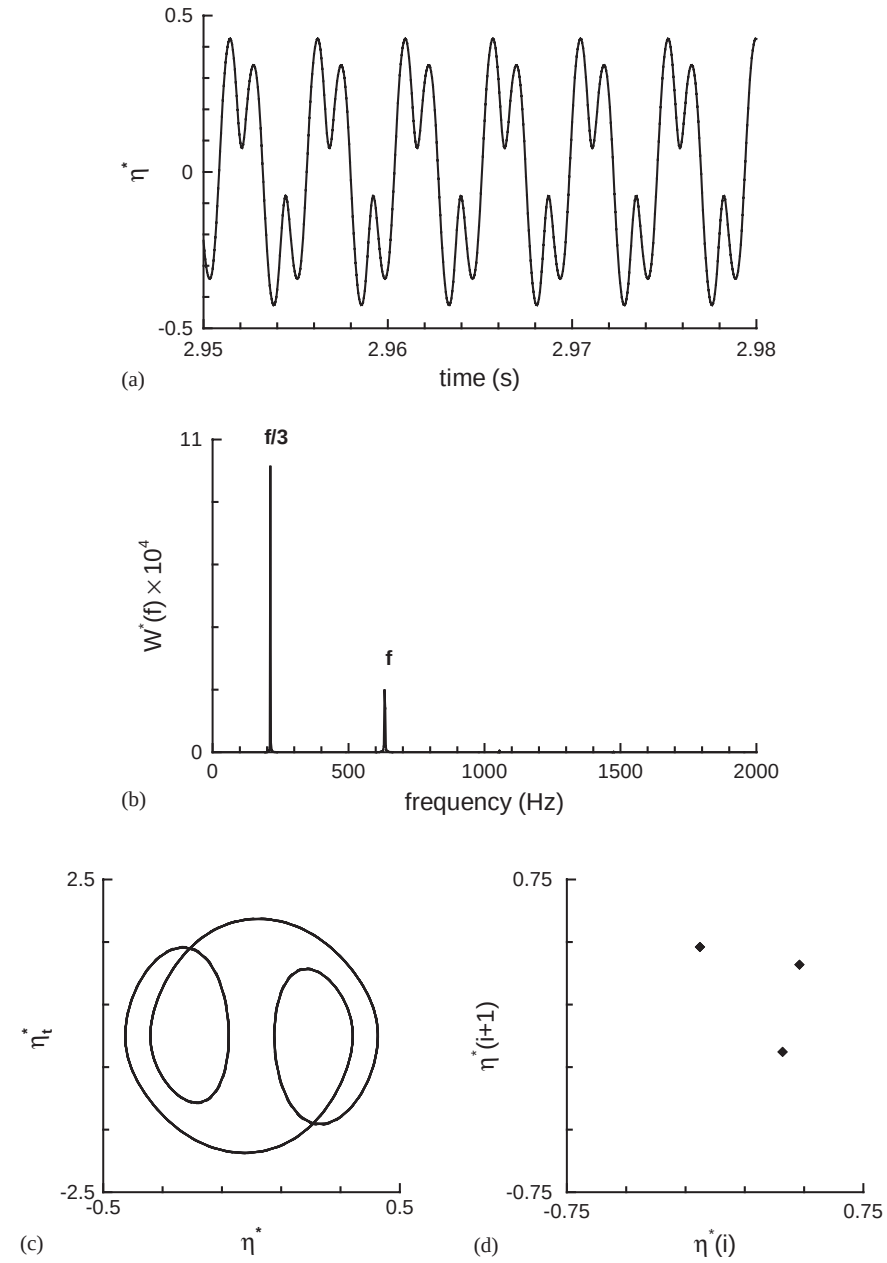

Fig. 10. Non-linear response of the beam center for $\varepsilon^* = 0.027$ and $\tau_w^* = 2.381$: (a) time history, (b) PSD, (c) phase diagram and (d) Poincaré map.

the beam damping. For this case, the value of Γ_t is increased and a sequence of solutions is obtained. Another passive technique consists of using the effect of low wall shear stress on the beam response (see Section 4.2). When control with a low τ_w^* is considered, the non-linear vibration (Eq. (1)) is solved for several low values of τ_w^*. The last control technique is an active one

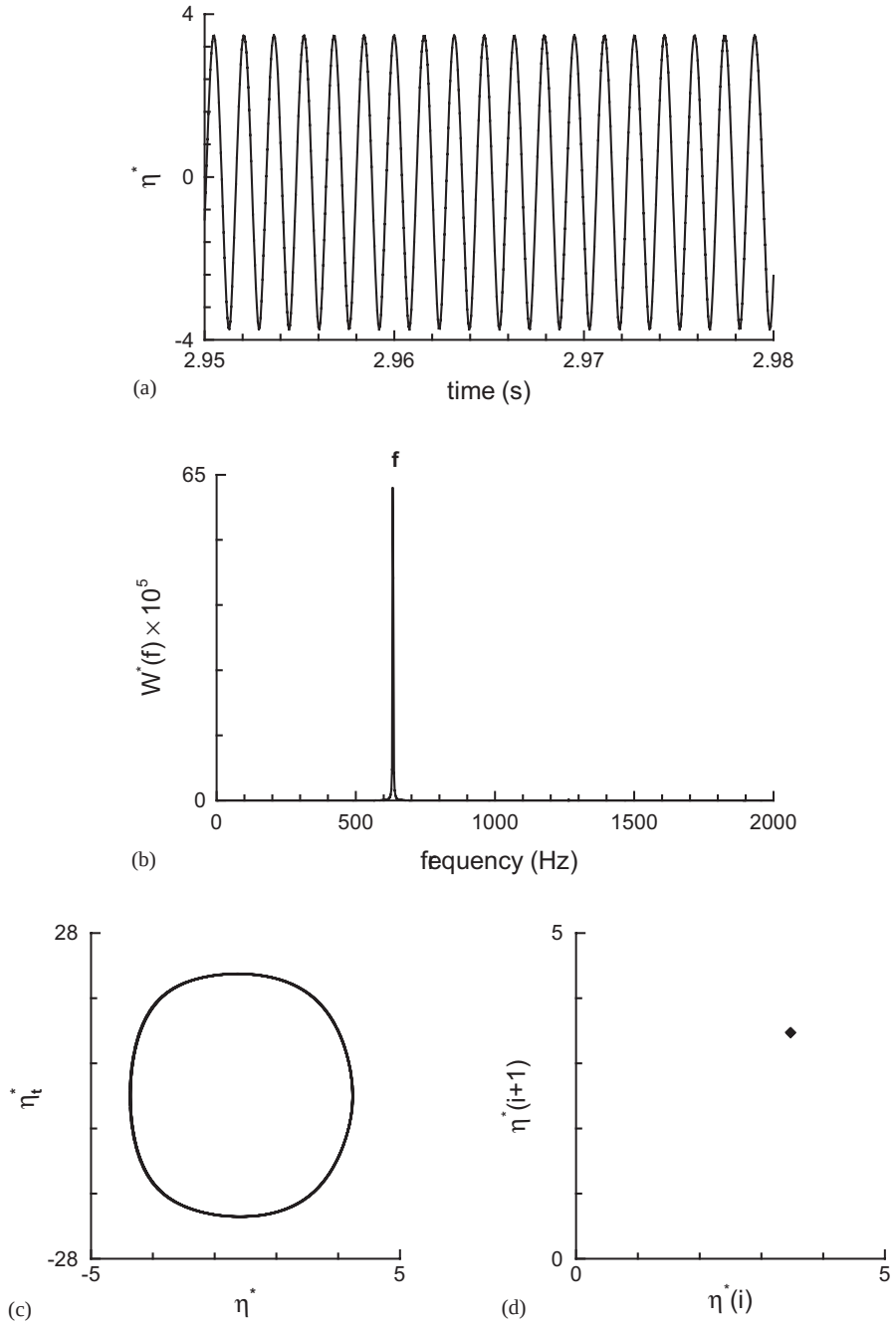

Fig. 11. Linear response of the beam center for $\varepsilon^* = 0.197$ and $\tau_w^* = 0.136$: (a) time history, (b) PSD, (c) phase diagram and (d) Poincaré map.

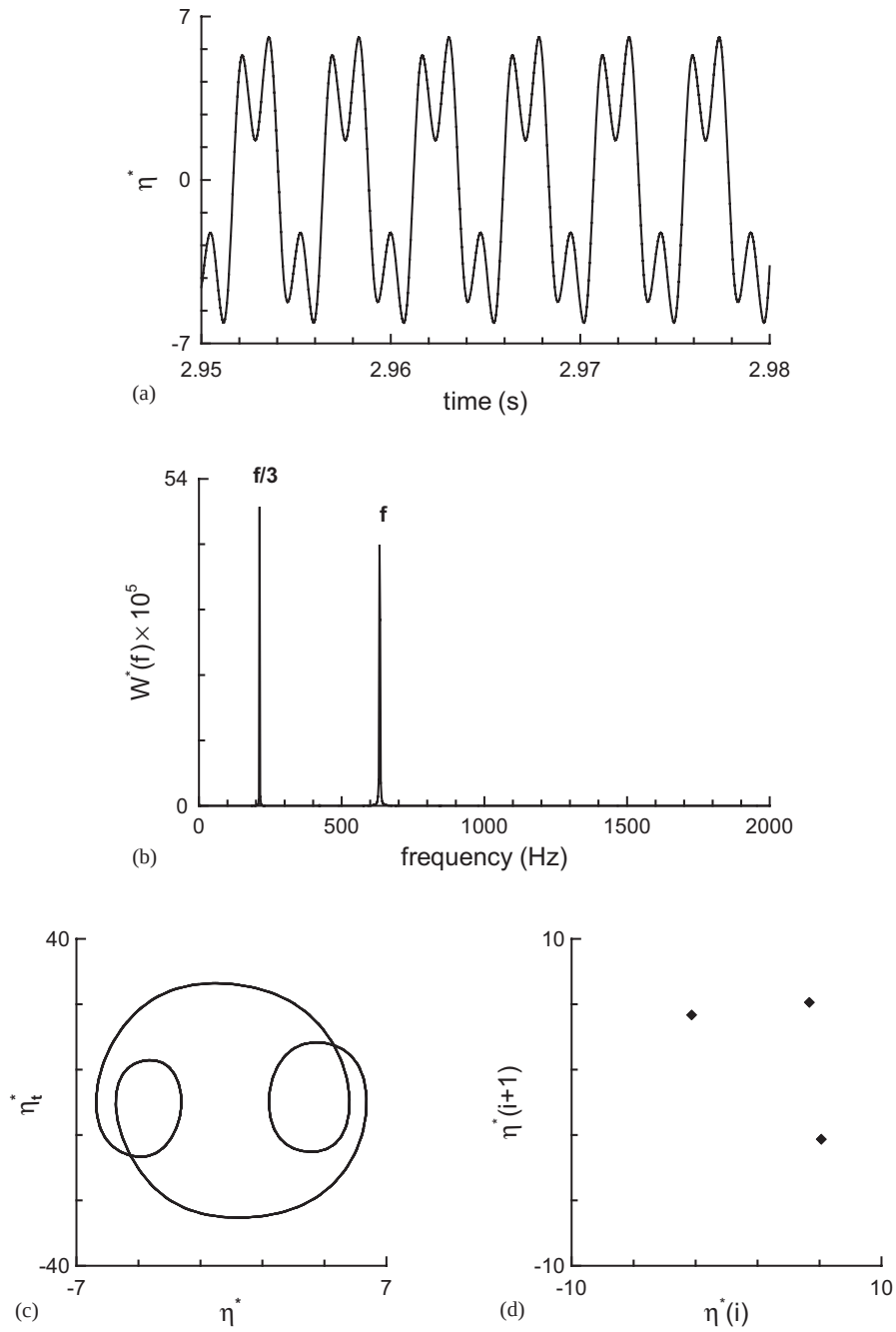

Fig. 12. Non-linear response of the beam center for $\varepsilon^* = 0.197$ and $\tau_w^* = 0.340$: (a) time history, (b) PSD, (c) phase diagram and (d) Poincaré map.

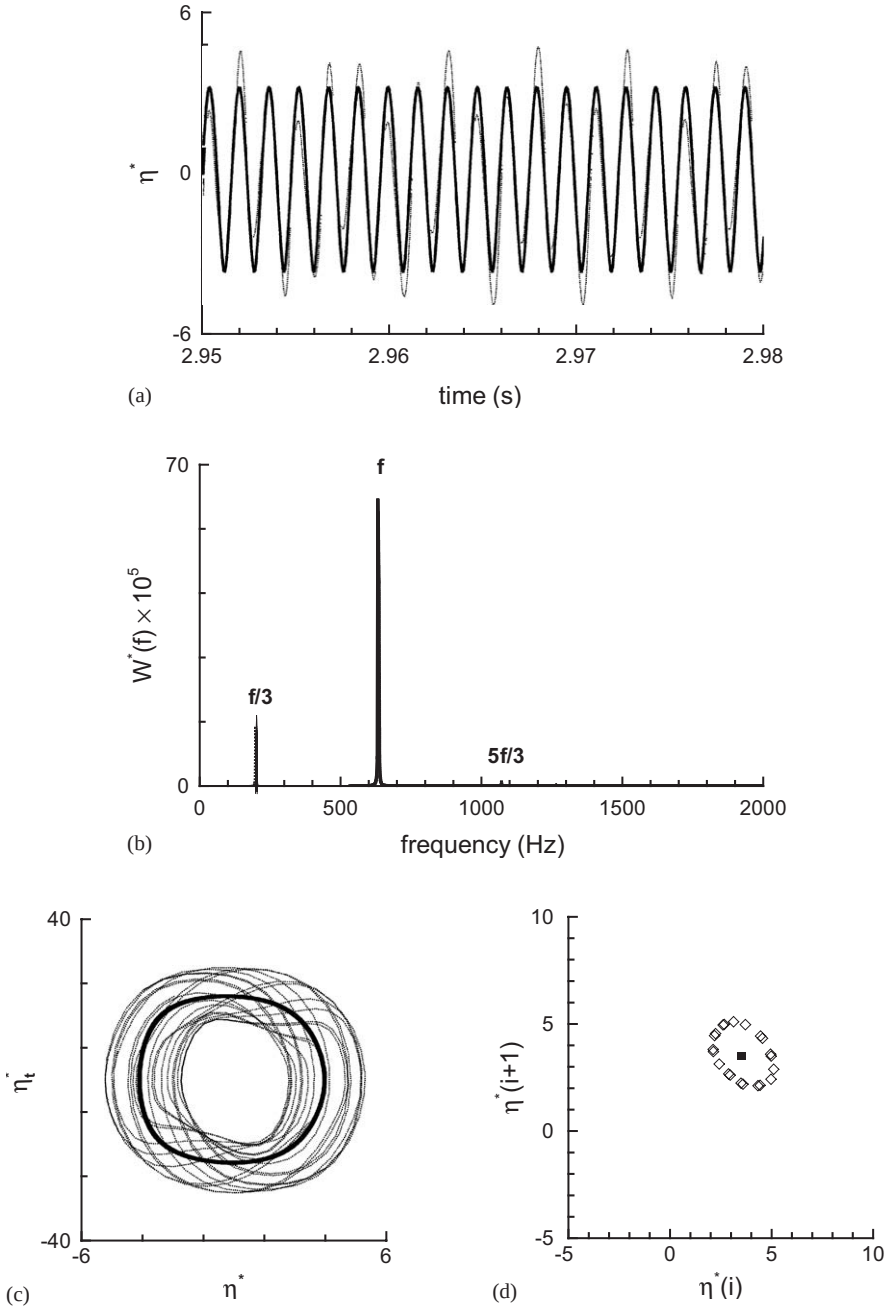

Fig. 13. Comparison of the response at the beam center (with and without control): (a) time history, (b) PSD, (c) phase diagram and (d) Poincaré map; ⋯, uncontrolled vibration; —, controlled vibration.

and simulates a shaker vibrating at the center of the beam at the same frequency as that of the excitation but with an opposite phase. For this case, solutions are obtained for different values of shaker excitation amplitude ε_s^*.

Results obtained for the damping tape, low shear stress and shaker methods are very similar. They show that, in all three cases, non-linear vibrations of the beam are reduced to linear-like vibrations. Since suppression of non-linear vibrations should be achieved with a minimum amount of energy, for each case the smallest value of the characteristic control term that suppresses the non-linear behavior is considered. For the first case of control with damping tape, suppression of non-linear vibrations is obtained for a minimum value of $\Gamma_t = 2.172 \times 10^2\,\mathrm{kg\,s/m^2}$. When control is applied using low shear stress, $\tau_w^* = 0.136$ is sufficient to suppress the non-linear behavior. However, this control is limited in the range of τ_w^* and as shown previously, when wall shear stress is increased to 0.340 the response becomes more non-linear. For the case of control with the shaker, a value of $\varepsilon_s^* = 0.068$ has to be reached in order to suppress the non-linear behavior. Fig. 13 shows the comparison between the uncontrolled response of the beam and the controlled response using the shaker method. The PSD, Fig. 13(b), shows that the $f/3$ subharmonic and the $5f/3$ harmonic are suppressed when control is applied to the beam. The phase diagram, Fig. 13(c), becomes also simpler since its shape is almost circular, whereas it had a more complex shape before control. This is confirmed by the Poincaré map, Fig. 13(d), which

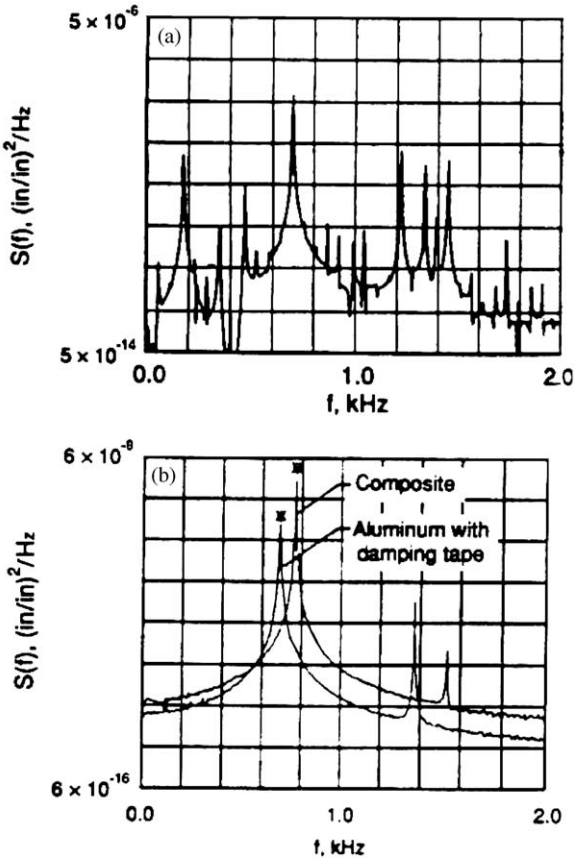

Fig. 14. Comparison of the strain response of a rectangular plate measured experimentally along its edge (see Ref. [6]): (a) uncontrolled and (b) controlled.

shows one point instead of the many points before control. The time history plot of the controlled response, Fig. 13(a), shows a linear-like response. The value of the maximum transverse displacement, although lower than the one of the uncontrolled responses, is still three times higher than the beam thickness. Fig. 14 shows experimental results obtained by Maestrello et al. [6] for a rectangular aluminum plate. Fig. 14(a) shows the power spectral density of the uncontrolled strain response, which shows a broadband response. Fig. 14(b) shows the power spectra of the controlled response for the case of a composite panel and that of an aluminum panel with damping tape. Both spectra of Fig. 14(b) show linear-like response. Our numerical results, though for a beam, are in good qualitative agreement with the experimental ones.

5. Conclusions

The non-linear structural vibrations of a beam subject to a harmonic excitation are studied and the effect of fluid wall shear stress is investigated. Various excitation amplitudes are tested and results show that in the non-linear vibration regime, energy is transferred from the fundamental to the harmonics and then to the subharmonics, as the excitation amplitude increases. The results show also the importance of wall shear stress in the non-linear model. For low excitation levels, large values of wall shear stress are required to trigger the non-linear response, which is characterized by an $f/4$ subharmonic bifurcation and a narrowband chaotic behavior. For high excitation levels, non-linear behavior is at first reduced (for small values of wall shear stress) then enhanced at high values of wall shear stress. Active and passive control techniques have been tested on the non-linear response and resulted in the recovery of the linear beam response. Energy is then transferred from the subharmonics and the harmonics back to the fundamental.

Acknowledgements

Support for this research was provided by the Office of Naval Research (ONR), under grant N00014-01-1-0128, with Dr. Luise Couchman as a technical monitor.

References

[1] M.M. Bennouna, R.G. White, The effect of large vibration amplitudes on the dynamic strain response of a clamped–clamped beam with consideration of fatigue life, Journal of Sound and Vibration 76 (2) (1984) 281–308.
[2] W.L. Starkey, S.H. Marco, Effects of complex stress time cycles on the fatigue properties of metals, Transactions of the American Society of Mechanical Engineers 79 (1957) 1329–1339.
[3] C. Mei, C.B. Prasad, Effects of non-linear damping on random response of beams to acoustic loading, Journal of Sound and Vibration 117 (2) (1987) 173–186.
[4] L. Maestrello, A. Frendi, Non-linear vibration and radiation from a panel with transition to chaos, American Institute of Aeronautics and Astronautics Journal 30 (11) (1992) 2632–2638.
[5] A. Frendi, L. Maestrello, A. Bayliss, Coupling between plate vibration and acoustic radiation, Journal of Sound and Vibration 177 (2) (1994) 207–226.
[6] L. Maestrello, A. Frendi, D.E. Brown, Non-linear vibration and radiation from a panel with transition to chaos, American Institute of Aeronautics and Astronautics Journal 30 (11) (1992) 2632–2638.

[7] W.L. Keith, J.C. Bennett Jr., Low-frequency spectra of the wall shear stress and wall pressure in a turbulent boundary layer, American Institute of Aeronautics and Astronautics Journal 29 (4) (1991) 526–530.
[8] D.M. Chase, A semi-empirical model for the wavevector-frequency spectrum of turbulent wall-shear stress, Journal of Fluids and Structures 7 (8) (1993) 639–659.
[9] C. Hoff, P.J. Pahl, Development on an implicit method with numerical dissipation from a generalized single-step algorithm for structural dynamics, Computer Methods in Applied Mechanics and Engineering 67 (2) (1988) 367–385.
[10] W. Buhler, Analysis and Suppression of Non-linear Beam Vibrations, Master Thesis, 2001.
[11] A. Frendi, Effect of wall shear stress on structural vibration, American Institute of Aeronautics and Astronautics Journal 39 (4) (2001) 737–740.
[12] A. Frendi, L. Maestrello, A. Bayliss, Coupling between plate vibration and acoustic radiation, Journal of Sound and Vibration 177 (2) (1994) 207–226.